Original article

Controlling factors and physical property cutoffs of the tight reservoir in the Liuhe Basin

Zhaozhao Tan[1,2], Weiming Wang[1]*, Wenhao Li[1], Shuangfang Lu[1], Taohua He[1,2]

[1] *Research Institute of Unconventional Oil & Gas and Renewable Energy, China University of Petroleum (East China), Qingdao, Shandong 266580, P. R. China*

[2] *School of Geosciences, China University of Petroleum (East China), Qingdao, Shandong 266580, P. R. China*

Abstract: Tight gas sandstone reservoirs of the Lower Cretaceous Xiahuapidianzi Formation are the main exploration target in the Liuhe Basin in China. Petrology characteristics, reservoir space (pore space), controlling factors and physical property cutoffs of the tight sandstone reservoir in the Liuhe Basin were determined through the integrated analysis of several methods including: casting thin section, field emission scanning electron microscopy (FE-SEM), X-ray diffraction (XRD), mercury intrusion porosimetry (MIP), nuclear magnetic resonance (NMR) and nitrogen gas adsorption (N_2GA). The sandstones dominated by lithic arkoses and feldspathic litharenites are characterized by low porosity, low permeability and strong microscopic heterogeneity. The porosity has a range between 0.48% and 4.80%, with an average of 2.26%. Intercrystalline pores, intergranular pores, dissolved pores and microfractures can be observed through the casting thin section and FE-SEM images. Compaction and carbonate cementation are the two primary mechanisms resulting in the low porosity of the Liuhe sandstones. Microfractures improve the permeability of the tight sandstones and provide pathways for fluid migration and the storage of hydrocarbon accumulations. Moreover, the theoretical cutoff of the porosity in the Xiahuapidianzi Formation tight sandstones is 3.3%.

Keywords: Reservoir space, controlling factors of physical properties, physical property cutoffs, water film, tight reservoir.

1. Introduction

There are many different geophysical methods to evaluate a reservoir, which include nuclear magnetic resonance logs, a full stack seismic inversion technique, sub-seismic techniques and borehole image logs (Chatterjee et al., 2012; 2013; 2017; Ou et al., 2015; Lai et al., 2017). Moreover, several analytical technologies for estimating an unconventional reservoir have also been widely applied, including thin section, field emission scanning electron microscopy (FE-SEM), mercury intrusion porosimetry (MIP) and nuclear magnetic resonance (NMR) (Wang et al., 2016a; Ge et al., 2017; Zhang et al., 2017). Controlling factors and physical property cutoffs are significant parts in reservoir evaluation, especially in a tight sandstone reservoir. Understanding the controlling factors and physical property cutoffs of tight reservoirs is beneficial to predictions of effective reservoir distribution and "sweet spot" (Zhu et al., 2009; Abdolmaleki et al., 2016). Predictive distribution of high-quality reservoirs in deeply buried

sandstone is a critical research area in siliciclastic diagenesis (Morad et al., 2000; Dutton and Loucks, 2010; Bjørlykke and Jahren, 2012; Zhou and Ji, 2016). Some scholars believed that sedimentation, diagenesis and tectonic activity played significant roles in controlling the physical properties of a tight reservoir (Ajdukiewicz and Lander, 2010; Maast et al., 2011; Lan et al., 2016). However, considering the strong microscopic heterogeneity of tight reservoirs, it is difficult to confirm the sweet zones of high porosity and permeability. Determining cutoffs is particularly important for prediction of a high-quality reservoir, as it represents the minimum threshold for oil and gas filling. Many different technologies have been used to discuss cutoffs of physical properties and to reveal the distribution characteristics of an effective reservoir, including the distribution function curve method, the empirical statistics method, the oil production test method, the irreducible water saturation method (Wang et al., 2011; Li et al., 2012), the porosity-permeability intersection method (Gao et al., 2010),
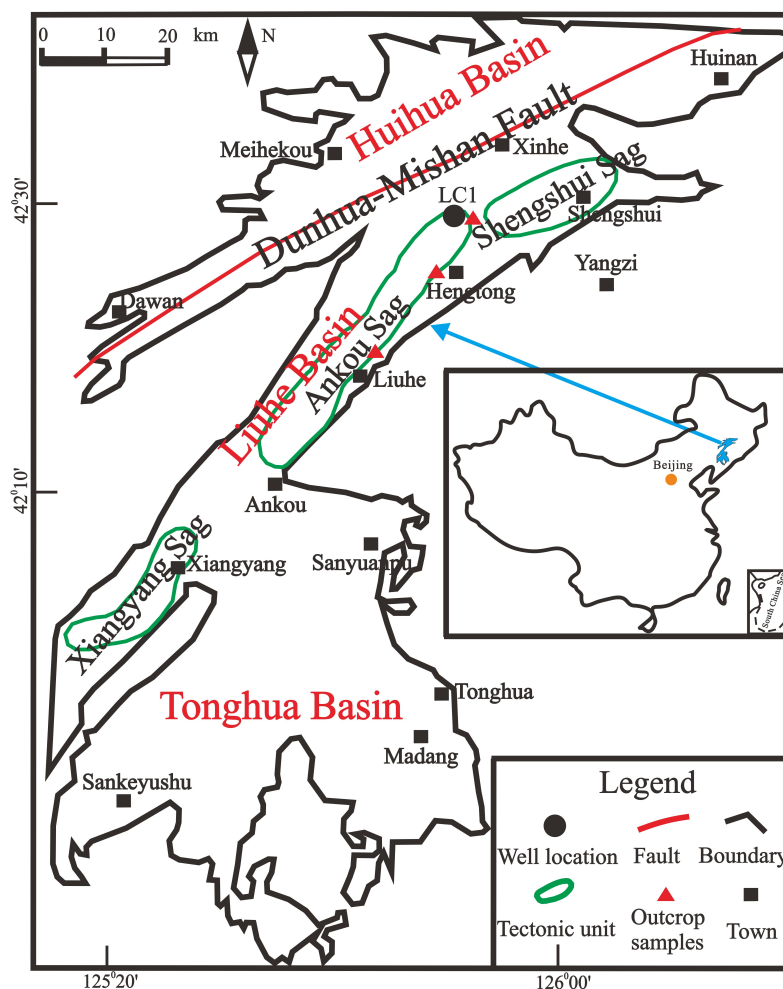

Fig. 1. Map showing the location and major structural elements of the Liuhe Basin.

the oil and gas displacement simulation method (Liu et al., 2012) and the minimum flowing pore throat radius method (Wu et al., 2016).

The Liuhe Basin is currently in the initial stages of exploration, with only one exploratory well (Well LC1). The Xiahuapidianzi Formation displays abnormal gas logging, and the sandstone reservoir has been filled by asphalt as seen under an optical microscope. There is no relevant research on this tight reservoir, thus the formation mechanism of the tight reservoir in the studied area remains unclear. For this reason, this study examined this reservoir utilizing a number of techniques, containing a casting thin section, FE-SEM, X-ray diffraction (XRD), MIP, NMR and nitrogen gas adsorption (N_2GA). Taking the Xiahuapidianzi Formation tight sandstone as an example, the reservoir space and controlling factors of the tight reservoir have been discussed. In addition, the theoretical cutoffs of physical properties also have been confirmed using water film thickness. In view of the low porosity and extra low permeability of the tight reservoir in the study area, this paper mainly focuses on the porosity. The research results of this article will be aimed towards understanding the storage mechanism of the tight reservoir in the Xiahuapidianzi Formation from the Liuhe Basin.

2. Geological setting

The Liuhe Basin is located between Dunhua-Mishan and the Yalujiang fault. It is adjacent to the north side of the Huihua Basin and south side of the Tonghua Basin (Shan et al., 2013). The basin is composed of five parts from north to south, and those parts are the western Slope Zone, the southern XinBin Uplift, the Shengshui Sag, the Ankou Sag and the Xiangyang Sag. Well LC1 is located between the Ankou Sag and the Shengshui Sag, closing to Dun-Mi fault (Fig. 1). The basin has undergone several active volcanic events (Xu et al., 2013). It developed cretaceous stratums including the Lamenzi Formation, the Dashatan Formation, the Baodaqiao Formation, the Xiahuapidianzi Formation and the Hengtongshan Formation from bottom to top. Affected by faults, Well LC1 only drilled into the Baodaqiao Formation, the Xiahuapidianzi Formation and the Hengtongshan Formation deposited by a lake-braided river delta sedimentary system (Fig. 2). Among these formations, the Xiahuapidianzi Formation provides the most favorable condition for oil generation and oil accumulation. Reservoirs develop primarily in the Xiahuapidianzi Formation, which consist of siltstones and fine-grained sandstones deposited in braided delta, lacustrine
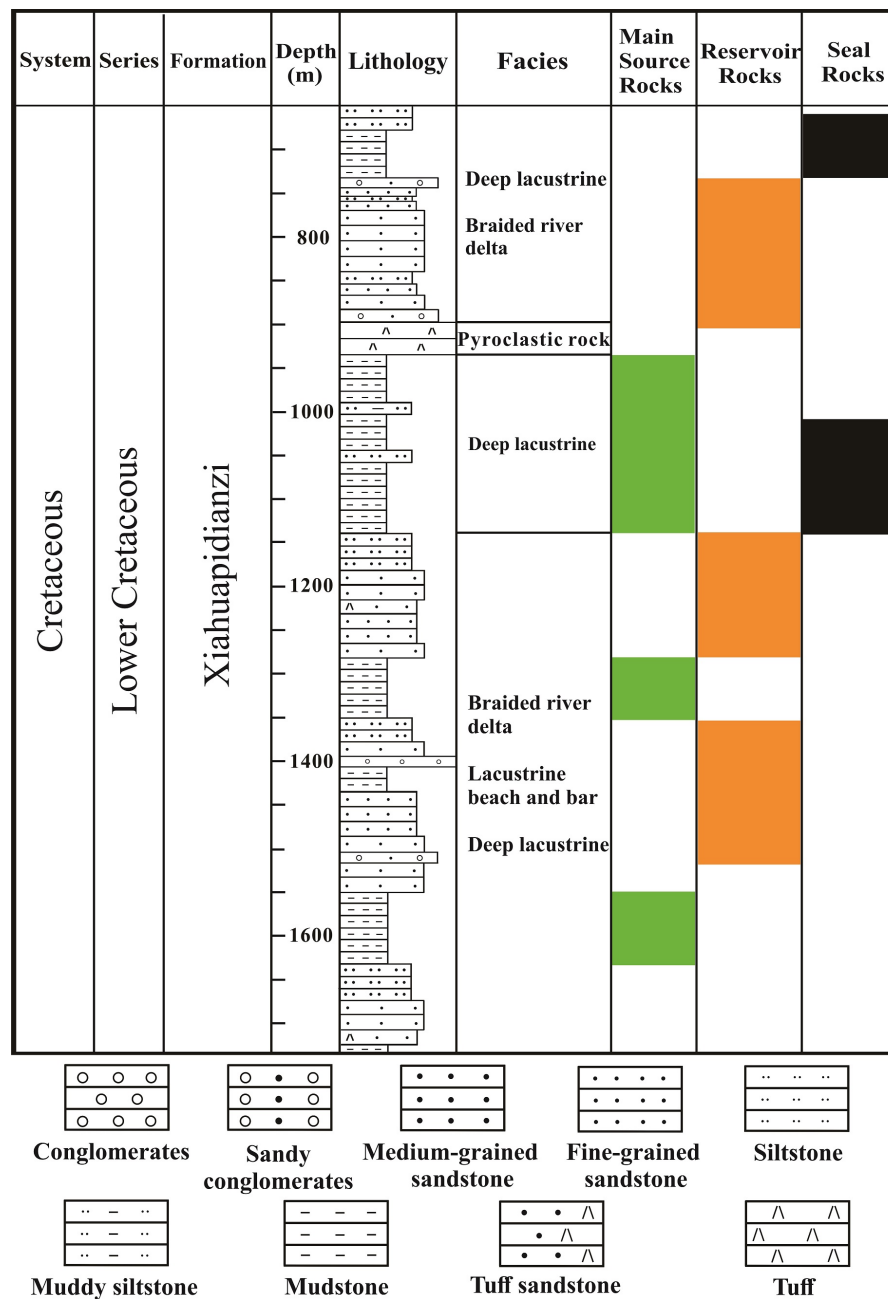
Fig. 2. Schematic stratigraphy and major source rocks, reservoirs and cap rocks in the Well LC1 from the Liuhe Basin.

and fan delta depositional systems (Fig. 2).

3. Materials and methods

Samples were taken from cores and outcrops. Continuous cores in the Xiahuapidianzi Formation were collected from Well LC1. Three outcrop samples were obtained from the Ankou Sag (Fig. 1).

3.1 Thin-section analysis

Thin-section petrography was performed to determine whole-rock mineralogy, diagenetic relationships and pore types. A total of 24 samples, impregnated with red epoxy under vacuum and stained with alizarin red-S and potassium ferricyanide (Dickson et al., 1966), were for thin sections analysis using a standard petrographic microscope.

3.2 Field emission scanning electron microscopy

FE-SEM was performed with a Quanta 200 F equipped with an energy-dispersive spectrometer on surfaces prepared by Ar-ion milling. Secondary electron images and backscattered electron images can provide important qualitative information on the general locations of pores throughout the sample. This experiment was conducted at 24°C and 35% humidity. A total of 27 samples from Well LC1 and the outcrop were selected for FE-SEM analysis.

3.3 X-ray diffractometry

To quantify the mineral content of the tight sandstones, 20 samples from Well LC1 and the outcrop were selected for whole-rock (bulk) and clay fraction (<2 μm) mineralogy using XRD. Preparation, analysis and interpretation procedures were modified from previously published procedures (Moor and Reynolds, 1997; Hiller, 2003).

3.4 Physical properties and other experimental analyses

Samples taken from Well LC1 and the outcrop (24 and 3, respectively) were measured for porosity and permeability analysis. The gas expansion method was utilized to determine porosity and helium was used as the measuring medium. Permeability was measured in a gas-autoclave using the pressure-transient technique and nitrogen was used as the permeating medium. Because the tight reservoir in the study area possessed such low permeability (K<0.1 mD), this paper focuses primarily on porosity instead of permeability. Other experiments (nitrogen gas adsorption (N_2GA), MIP and NMR) were also performed on the samples. The N_2GA experiments were performed using a Quadrasorb SI surface area and pore size analyzer obtained from Quantachrome Ins. Before analysis, the crashed samples (60-80 mesh) were degassed in a vacuum drying oven at 250°C for 12 h to eliminate both capillary water and irreducible water (Chen et al., 2015). The amount of adsorbed gas was measured by a static volumetric method at the subcritical temperature (77 K). A multi-point Brunauer-Emmett-Teller (BET) (Brunauer et al., 1938) model was used to analyze the N_2GA experimental data to determine the specific surface area. Rock density parameters in this study are from MIP experiments. The MIP was performed using an Autopore III 9420 Instrument (Micrometrics, USA) by the SY/T 5346-2005. Preparation, analysis and interpretation procedures of the MIP are referenced from Zhang (2017). Irreducible water saturation parameters in the article are from NMR experiments using the T_2 cutoff method (Yao et al., 2010). The RecCore-2500 low field magnetic resonance tester of the Institute of the Fluid Flow Mechanics of the Chinese Academy of Science, in Langfang City, was used in this research.

3.5 Cutoff of physical property analysis

There is water on the interface layer of the liquid-solid two-phase system. It is called water film and adsorbed on the surface of the solid phase. Water film can also be formed by reservoir water on the surface of rock particles (Bohr et al., 2010; Nishiyama et al., 2013). The existence of water film can reduce the effective radius of the pore throat and influence seepage of stratum fluids (Tokunaga, 2011). The rock particles of tight reservoir are fine and have high content of clay minerals charged negatively. Water is highly polar and it can form a static electric field on the surface of rock particles, causing a specific arrangement of water molecules (Wang et
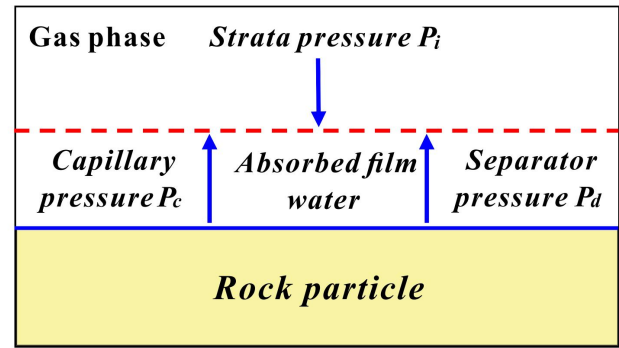

Fig. 3. Schematic showing the forces working on the water film.

al., 2006). In theory, the adsorption capacity of water binding with the surface sandstone particles becomes weaker from the inside out. The water molecules attached directly to the rock surfaces are strongly bound due to electrostatic and van der Waals forces, which lead to the fact that they cannot migrate or dissolve other particles (Derjaguin et al., 1974).

Due to the close arrangement of particles, there would be no free water in the throat, only an absorbed water film around the throat. It is difficult for natural gas to displace adsorbed water. When the throat radius is less than the water film thickness, water saturates its corresponding pore throat radius and pore space. In this circumstance, oil and gas cannot experience secondary migration. Therefore, the water film thickness represents the lower limit of the critical pore throat radius in certain strata conditions (Staszczuk, 1995; Wang et al., 2012).

Force balance analyses of water film in tight sandstone samples reveal the generation mechanisms of the film. The water film tightly aligns to the surface of solid particles due to the polar nature of water. Three forces are working on it: P_d (separation force), P_i (formation hydrostatic pressure) and P_c (capillary force) (He et al., 1998; Zhang et al., 1998; Wang et al., 2012). When pressed by an external force, the film thins out and experiences P_d. P_i is the force pointing vertically towards the surface of the sand particles. P_c is the capillary force which is the opposite force of P_i. Fig. 3 shows the force analysis of water film and ignores gravity. The pressure formula of the water film can be expressed as:

$$P_i = P_d + P_c \tag{1}$$

The pressure difference between the two interfaces (solid and gas) of the film is called the capillary pressure P_c and depends on the interfacial tension between gas and water, the capillary diameter and the wettability of the medium:

$$P_c = \frac{2\sigma cos\theta}{r} \tag{2}$$

where r is the throat radius (μm); θ refers to the contact angle and σ is the interfacial tension between water and gas (N/m).

Elliptic polarization of light technology has been applied to determine water film thickness, which attaches to the hydr-
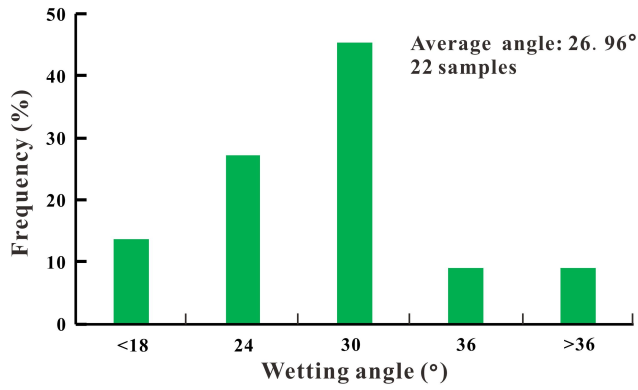
Fig. 4. Distribution of wetting angles.

Fig. 5. Relationship between the water film thickness and the throat radius in different formation pressures.

ophilic silica surface under different separation pressures. The equations of separator pressure (P_d) are readily obtained based on acquiring the appropriate measurements (Gee et al., 1990):

$$P_d = \frac{2200}{h^3} + \frac{150}{h^2} + \frac{12}{h} \tag{3}$$

Based on equations (1), (2) and (3), the relationship between the critical thickness of the water film and throat radius is described by:

$$r = \frac{2\sigma \times cos(\theta \times \frac{\pi}{180})}{(P_i - \frac{2200 \times 10^{-10}}{h^3} - \frac{150 \times 10^{-6}}{h^2} - \frac{0.12}{h})} \tag{4}$$

where h is the thickness of water film, μm; σ is the interfacial tension between the gas and water, N/m; P_i is the strata pressure, MPa; r is the throat radius, μm; θ is the wetting angle.

4. Results

4.1 Cutoff of physical property

4.1.1 Selection of Key Parameters

The wetting angle of tight sandstone was measured with a Model LT/Y2009-005 contact angle meter and determined with pendant-drop experiments on 22 samples. The measurements (Fig. 4) show that tight sandstone samples are strongly water-wet and have varying wetting angles but mostly range between 18° and 30°. We used a mean value of 26.96° in our calculations. Usually, gas/water interfacial tension decreases as pressure and temperature increases. However, the methane/water interfacial tension does not follow the pattern and remains at approximately 0.03 mN/m (Bao et al., 1988) when the formation pressure is higher than 25 MPa and the temperature is higher than 95°C.

4.1.2 Determination of water film thickness

Utilizing the wetting angle, the gas/water interfacial tension, and equation (4), this paper established the relationship between the throat radius (r) and the water film thickness (h) of the tight reservoir under different formation pressures (Fig. 5). The red imaginary line "Y = X" represents "water film th-
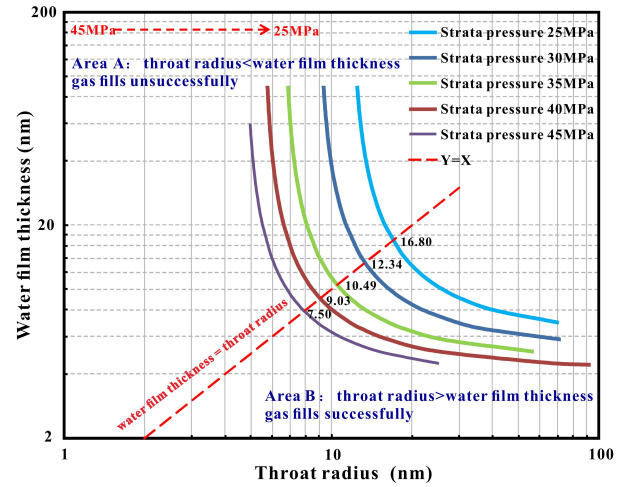
ickness = throat radius". In the bottom right of "Y = X" (Area B), it shows that the throat radius exceeds the water film thickness and natural gas fills successfully. Conversely, Area A illustrates the failure of gas filling.

The critical condition of a tight reservoir cutoff is established when the water film thickness equals the throat radius. The throat is completely filled with bound water instead of natural gas. Fig. 6 shows the critical water film thickness under different formation pressures (Table 1).

Table 1. Critical water film thickness in different formation pressures.

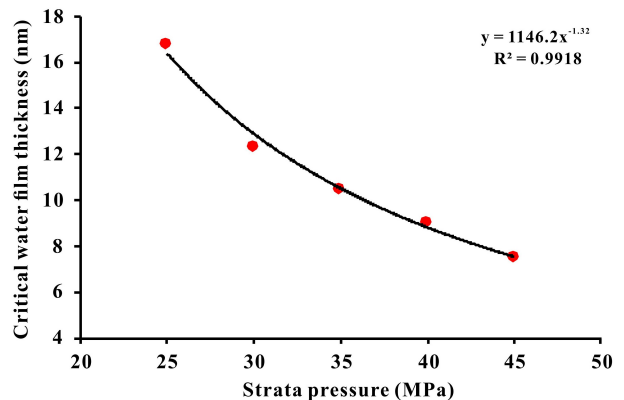| Depth (m)	Strata pressure (Mpa)	Critical water film thickness (mm)
2500	25	16.80
3000	30	12.34
3500	35	10.49
4000	40	9.03
4500	45	7.50

Fig. 6. Relationship between water film thickness and strata pressure.

Table 2. Cutoffs of porosity in Well LC1 calculated by the water film thickness method.

Well	Original depth, (m)	Strata pressure, (Mpa)	Specific surface area, (m²/g)	Irreducible water saturation, (%)	Critical water film thickness, (nm)	Rock density, (g/cm³)	Porosity cutoffs, (%)
LC1	2846.6	28.46	5.78	82.71	14.00	2.87	3.94
LC1	2847.4	28.47	3.91	77.15	13.99	2.69	2.67
LC1	3150.0	31.50	6.37	87.94	12.13	2.68	3.29

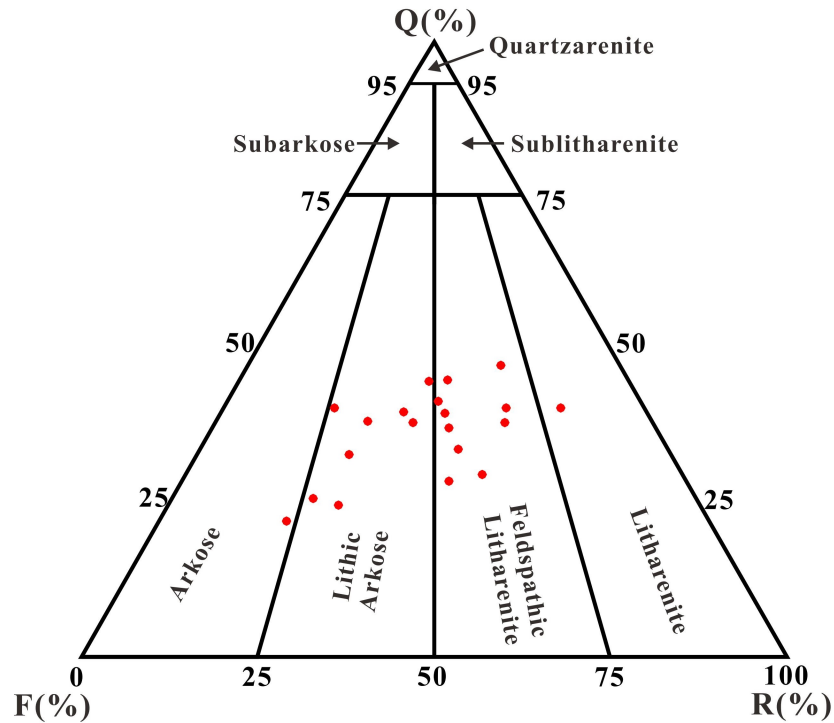*Note: Original depth consists of current depth and denudation thickness (1700m).*

Fig. 7. Classification of the Liuhe tight sandstone samples using Folk's (1980) classification.

4.1.3 Determination of porosity cutoff

Based on the results shown in Table 1, the relation between strata pressure and critical water film thickness can be established (Fig. 6). The water film thickness, porosity and bound water saturation have the following relationship (Zou et al., 2011);

$$H = \frac{71.42\Phi \times S_{wi}}{(A \times \rho)} \quad (5)$$

and the porosity may be calculated:

$$\Phi = \frac{h \times A \times \rho}{(71.42 \times S_{wi})} \quad (6)$$

where h is the thickness of bound water film, nm; Φ is the porosity of rocks, %; S_{wi} is the saturation of bound water (obtained from NMR), %; A is the specific surface area of rock (BET specific surface, obtained from N_2GA), m²/g; ρ is the skeleton density rocks, kg/m³ (obtained from MIP).

Inserting the critical water film thickness and the bound water saturation into equation (6), the cutoffs of porosities in different strata pressures can be calculated (Table 2).

The denudation thickness determined by vitrinite reflectance method was 1700 m in the Liuhe Basin, therefore, the original depth was 2350 m to 3450 m in the Xiahuapidianzi Formation. Because the maximum depth can reach up to 3450 m in the Xiahuapidianzi Formation, the reservoir is very tight with theoretical porosity cutoff of 3.3%. Most measured porosities are less than the theoretical cutoff in the lower Xiahuapidianzi Formation. Porosities higher than 3.3% are located primarily in the upper Xiahuapidianzi Formation (650 m∼800 m).

4.2 Petrology characteristics of tight sandstone

The tight sandstones in the Xiahuapidianzi Formation are classified mainly as lithic arkoses and feldspathic litharenites according to Folk's classification scheme (1980) (Fig. 7). Detrital components contain between 25.3% and 54.7% quartz (mostly monocrystalline) with an average of 41.80%. Rock fragments have a range of 12.60% to 44.80% with an average of 27.43%. The rock fragments are mainly igneous in origin, with subordinate amounts of sedimentary rocks and

Table 3. Average composition of detrital diagenetic and point-count porosity of the samples from well LC1 and outcrop in Liuhe Basin.

Well	Depth/m	Lithology	Grain			Matrix	Cement	Φ/%	Authigenic clay minerals (XRD)						C /% (XRD)	Point counting porosity in thin section or SEM		
			Q/%	F/%	RF/%				Total clay	Ill	Kln	Chl	I/S	C/S		IGP /%	SP /%	MF /%
Outcrop1	/	S	46.6	8.6	44.8	18.0	5.1	3.45	37.0	45.0	0.0	37.0	18.0	0.0	3.9	2.2	0.0	/
Outcrop2	/	S	54.7	13.2	32.1	10.0	5.9	2.16	17.8	50.0	13.0	30.0	7.0	0.0	5.5	1.7	0.3	/
Outcrop3	/	FS	46.7	16.4	36.9	16.0	5.0	3.21	34.0	36.0	0.0	49.0	15.0	0.0	4.8	1.9	0.0	/
LC1	736	CS	44.0	31.0	25.0	15.0	8.7	3.66	10.6	38.0	10.0	40.0	10.0	2.0	8.3	2.6	0.1	0.75
LC1	748	FS	34.1	26.0	39.9	9.0	5.5	4.60	28.8	28.0	0.0	53.0	7.0	12.0	4.6	3.0	0.0	/
LC1	752	FS	28.5	49.2	22.3	10.2	6.6	4.30	19.0	35.0	15.0	29.0	12.0	9.0	6.3	2.1	0.2	/
LC1	759	S	29.7	52.3	18.0	7.5	5.4	2.22	7.9	28.0	0.0	40.0	16.0	16.0	4.9	1.8	0.1	0.6
LC1	780	MS	38.0	43.0	19.0	8.8	3.5	4.80	8.6	41.0	0.0	38.0	18.0	3.0	3.0	3.1	0.5	/
LC1	790	MS	52.0	22.0	26.0	10.0	3.1	4.10	9.2	43.0	0.0	47.0	16.0	0.0	2.8	2.9	0.3	/
LC1	825	S	39.0	27.0	34.0	6.7	2.5	3.01	8.8	45.0	0.0	40.0	15.0	0.0	2.2	1.4	0.0	/
LC1	847	FS	44.0	17.9	38.1	11.3	27.6	0.68	10.9	7.0	0.0	75.0	0.0	18.0	27.1	0.4	0.0	0.4
LC1	865	S	/	/	/	/	/	1.76	/	/	/	/	/	/	/	/	/	/
LC1	885	MS	46.7	40.7	12.6	6.4	6.8	2.22	10.0	57.0	0.0	33.0	0.0	10.0	5.2	1.0	0.2	0.8
LC1	1027	FS	41.3	39.2	19.5	6.8	8.8	1.87	12.3	41.0	0.0	32.0	15.0	12.0	7.8	1.1	0.0	/
LC1	1039	FS	44.2	37.3	18.5	7.0	7.6	2.56	15.4	43.0	0.0	26.0	10.0	21.0	5.9	1.2	0.1	0.5
LC1	1146.6	S	45.7	25.5	28.8	12.0	11.3	1.62	26.0	37.0	0.0	63.0	0.0	0.0	10.9	1.2	0.3	/
LC1	1147.4	S	47.9	25.3	26.8	15.5	8.8	2.84	24.6	48.0	0.0	52.0	0.0	0.0	5.0	1.6	0.0	/
LC1	1148.8	S	42.9	26.4	30.7	13.0	10.7	2.51	18.0	49.0	0.0	51.0	0.0	0.0	8.3	1.2	0.3	/
LC1	1150.1	FS	32.9	31.4	35.7	10.2	17.1	0.85	20.0	51.0	8.0	31.0	10.0	0.0	14.3	0.5	0.0	0.42
LC1	1150.55	FS	51.7	24.8	23.5	12.6	18.9	0.74	14.7	41.0	0.0	59.0	0.0	0.0	15.0	0.4	0.0	0.58
LC1	1220	FS	/	/	/	/	/	1.96	/	/	/	/	/	/	/	/	/	/
LC1	1237	S	/	/	/	/	/	2.37	/	/	/	/	/	/	/	/	/	/
LC1	1351.6	S	/	/	/	/	/	1.49	/	/	/	/	/	/	/	/	/	/
LC1	1385.1	FS	/	/	/	/	/	1.49	/	/	/	/	/	/	/	/	/	/
LC1	1400	CS	25.3	58.2	16.5	4.0	16.8	0.68	8.7	33.0	0.0	59.0	0.0	8.0	13.1	0.3	0.0	0.38
LC1	1450	FS	/	/	/	/	/	1.73	/	/	/	/	/	/	/	/	/	/
LC1	1655	S	/	/	/	/	/	1.10	/	/	/	/	/	/	/	/	/	0.5

Q, quartz; F, feldspar; RF, rock fragment; Φ, measured porosity; Ill, illite; Kln, kaolinite; Chl, chlorite; I/S, mixed-layer illite-smectite; C/S, mixed-layer chlorite-smectite; C, carbonate; (the content of Ill, Kln, Chl, C/S, I/S and carbonate are measured from XRD); IGP, intergranular porosity; SP, secondary porosity; MF, microfracture; S = Siltstone; FS = Fine-grained sandstone; CS = Coarse-grained sandstone; MS = Medium-grained sandstone; / represents no data.

metamorphic rocks. Feldspar content varies from 8.60% to 58.20% with an average of 30.77% (Table 3) and consists of both plagioclase and K-feldspar. The average grain size in these samples varies from 0.025 to 1.0 mm. The grains contain both subangular and subrounded shapes, and the grains are moderately to poorly sorted. Generally, the Xiahuapidianzi Formation tight sandstones are mineralogically immature reservoirs with low textural maturity.

4.3 Pore types of reservoir space

The thin section and FE-SEM data show that the reservoir in the Xiahuapidianzi Formation is extremely tight. Intergranular pores, intercrystalline pores and dissolved pores can be observed in some samples. Moreover, microfractures with an aperture of less than 0.1 mm (Anders et al., 2014; Lai et al., 2017) are widely distributed in the Xiahuapidianzi Formation.

The intergranular pores are only observed under a microscope due the influence of sedimentation and diagenesis (The intergranular pores were likely shrunk by mechanical compaction and cementation). They occur predominantly around three mineral grains, quartz, feldspar and clay minerals (Fig. 8a, b). The intercrystalline pores are common in the tight reservoir with the pore sizes from 0.1 to 1 μm. This type of pore develops primarily in clay mineral particles (Fig. 8c) and in calcite grains (Fig. 8d). Dissolution can significantly impact the physical properties of the tight reservoir. However, dissolution in the study area is not obvious and is seldom observed in feldspar particles (Fig. 8e, f) or rock
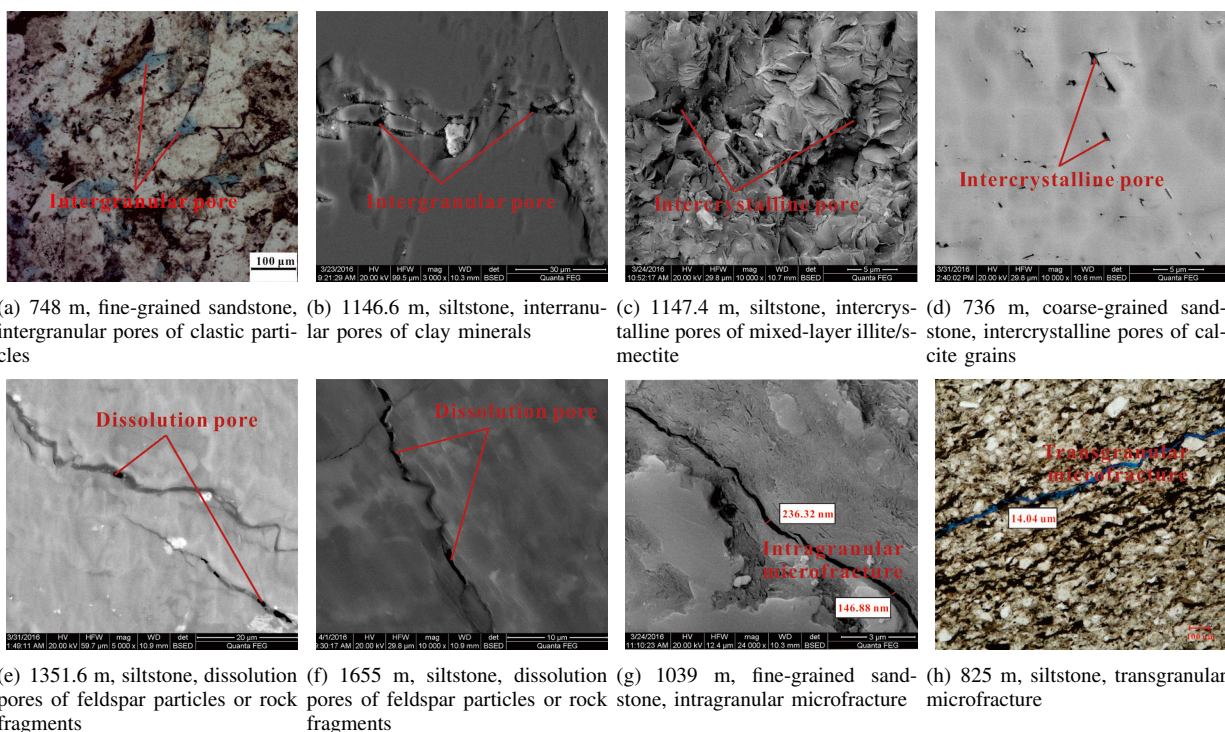
(a) 748 m, fine-grained sandstone, intergranular pores of clastic particles

(b) 1146.6 m, siltstone, interranular pores of clay minerals

(c) 1147.4 m, siltstone, intercrystalline pores of mixed-layer illite/smectite

(d) 736 m, coarse-grained sandstone, intercrystalline pores of calcite grains

(e) 1351.6 m, siltstone, dissolution pores of feldspar particles or rock fragments

(f) 1655 m, siltstone, dissolution pores of feldspar particles or rock fragments

(g) 1039 m, fine-grained sandstone, intragranular microfracture

(h) 825 m, siltstone, transgranular microfracture

Fig. 8. Reservoir space types of a tight reservoir in the Xiahuapidianzi Formation from Well LC1 in the Liuhe Basin.

fragments. Microfractures are widely distributed in the tight reservoir, including both intragranular microfractures (Fig. 8g) and transgranular microfractures (Fig. 8h). The existence of these microfractures provides channels for fluid migration and also improves reservoir properties to a certain extent.

4.4 Diagenesis and authigenic mineralogy

The burial history indicates that the Liuhe Basin was in a period of rapid subsidence during the late Cretaceous. The sandstones suffered from significant mechanical compaction, which commonly resulted in intergranular volume (IGV) loss. The mechanical compaction can be identified by the following phenomenon: the orientation arrangement in the long axis of clastic particles (Fig. 9a) and the dominance of linear and concave-convex grain contacts (Fig. 9a, b). Samples without extensive eogenetic cements suggest that the deterioration of porosity is mainly caused by mechanical compaction (Fig. 9b).

The dissolution in the study area focuses on feldspar and lithic debris particles (Fig. 9c, d), but it is not obvious. The dissolution porosity ranges between 0.1% and 0.5% based on thin section images (Table 3). Compared with the dissolution of feldspars grains and lithic fragments, the dissolution of pore-filling cements (e.g., calcite) is less common in the sandstones. Typically, secondary dissolution pores are frequent in microfractures (Fig. 8e, f).

Almost all tight sandstones underwent various levels of cementation. The major minerals of the cements are carbonate (e.g., calcite and ferro-calcite) and authigenic clay (e.g., illite, illite/smectite and chlorite). Carbonate minerals, including calcite and ferro-calcite, are the prevalent cements in the

Liuhe sandstones. It is observed that many feldspar and lithic fragments are replaced by carbonate mineral during diagenesis (Fig. 9e, f, g). Calcite is the predominant cement in the samples from shallow to deep and either partially or completely fill the pore space (Fig. 9e, g).

Total clay content as measured by XRD varied between 8.60% and 37.0%, with an average of 17.8% (Table 3). XRD data also revealed that the clay minerals in these samples are illite (from 7.0% to 57.0% with an average of 39.4%), kaolinite (from 0 to 15.0% with an average of 2.6%), chlorite (from 6.0% to 63.0% with an average of 43.8%), mixed-layer illite/smectite (I/S) (from 0 to 18.0% with an average of 7.7%) and mixed-layer chlorite/smectite (C/S) (from 0 to 21.0% with an average of 5.5%). The authigenic clay cements in the Liuhe sandstones are present primarily as chlorite and illite, both of which filled the intergranular pores (Fig. 9h, i).

5. Discussion

### 5.1 Diagenetic controls on reservoir quality

There are two main types of diagenesis in the sandstone reservoir. One is destructive diagenesis which consists of compaction, cementation and metasomatism (Maast et al., 2011; Lai et al., 2015; Aretz, et al., 2016). These destructive diageneses not only reduce the primary porosity of reservoir but also further destroy secondary solution pores. The other type of diagenesis is constructivedigenesis, and the main form of that is dissolution. Dissolution can promote improvement of the reservoir space and enhance the storage capability of reservoir to a limited extent (Taylor et al., 2010). Through microscopic observation, the diagenesis in the study area
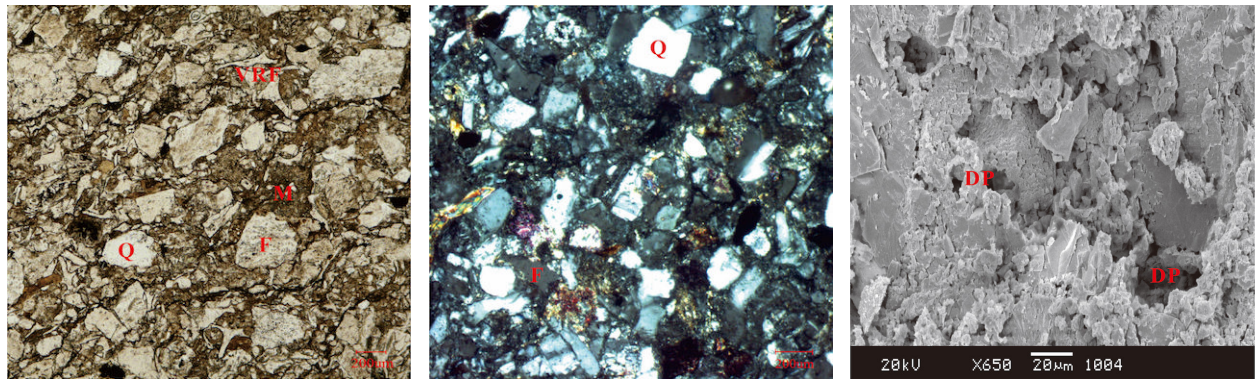
(a) 1220 m, fine-grained sandstone, subrounded to subangular, poorly sorted, orientation arrangement of the long axis of clastic grain due to the strong compaction

(b) 1039 m, fine-grained sandstone, subrounded to subangular, poorly sorted, linear grain contacts and concaveconvex grain contacts

(c) 790 m, medium-grained sandstone, dissolution pores occurring around feldspar grains
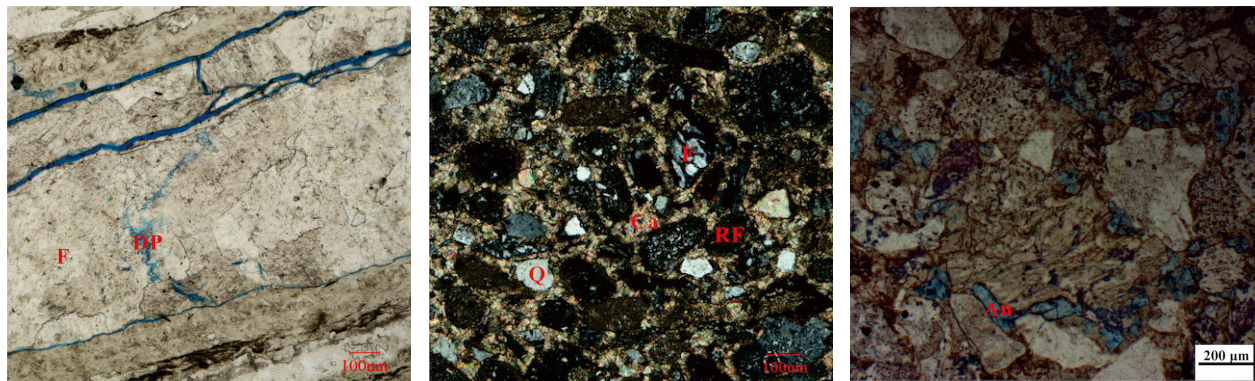
(d) 1528 m, coarse-grained sandstone, dissolution pores of feldspar grains

(e) 1450 m, fine-grained sandstone, subrounded to subangular, poorly sorted, crystal cementation of calcite

(f) 1385.1 m, fine-grained sandstone, subrounded to subangular, poorly sorted, mosaic cementation of calcite
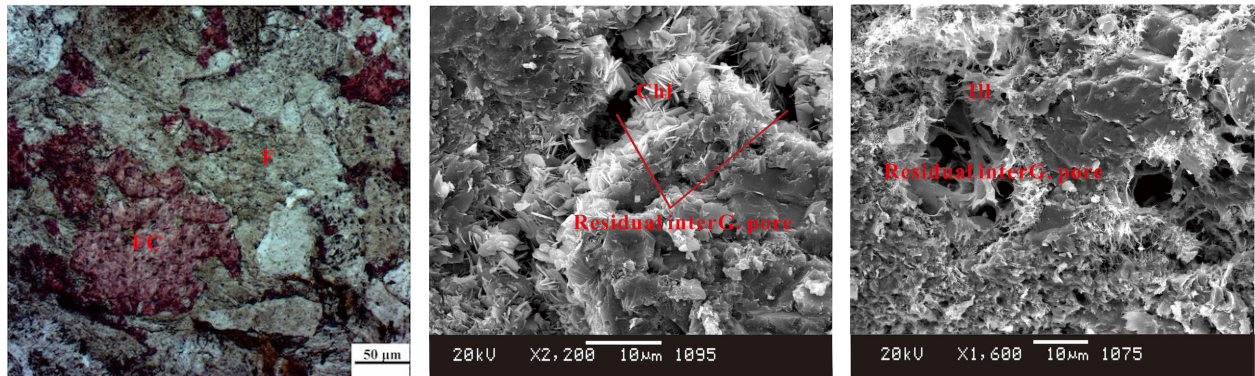
(g) 1139 m, medium-grained sandstone, subrounded to subangular, poorly sorted, feldspar replaced by ferro-calcite

(h) Outcrop-1, siltstone, chlorite filling the intergranular pores

(i) 1351.6m, siltstone, illite filling the intergranular pore

Fig. 9. Diagenesis types of the tight reservoir in the Xiahuapidianzi Formation from Well LC1 in the Liuhe Basin. Q = quartz; F = feldspars; M = matrix; RF = rock fragments; Ca = calcite; FC = ferro-calcite; An = ankerite; VRF = volcanic rock fragments; DP = dissolution pores; interG. pore =intergranular pore; Chl = chlorite; Ill = illite.

appears to be more destructive than constructive diagenesis.

5.1.1 Compaction

Compaction is one of the important mechanisms that causes loss of reservoir porosity, especially in the early stages of diagenesis (Paxton et al., 2002). The strong mechanical compaction leads to closer packing of the framework grains, which greatly reduces the primary porosity (Paxton et al., 2002; Aretz et al., 2016). During deposition period of the Xiahuapidianzi Formation, the basin was in a period of rapid subsidence. The sandstones suffered from strong compaction, which caused a dramatic loss of porosity. In the western Laiyang Sag of the Jiaolai Basin in Eastern China, the rocks are primarily feldspathic litharenites that underwent progressive burial. The primary porosity is partially to completely eliminated as a result of significant mechanical compaction of the ductile grains (Zhou et al., 2016). Similarly, the XRD results indicate that Liuhe sandstones have a high content of plastic minerals (clay minerals; Table 3) and a low brittle mineral content (quartz, feldspar, etc.; Table 3). This shows a weak ability to resist compaction and does not favor primary pore preservation. Although characterized by intense homogeneity, the reservoir quality of Liuhe sandstone varies at different burial depths. Fig. 10 shows that porosity gradually decreases as the depth increases. Samples at the burial depth of 800 m in the upper Xiahuapidianzi Formation have high porosities (with an average of 3.95%), whereas samples at the burial depth of 1400 m in the lower Xiahuapidianzi Formation have low porosities (with an average of 1.35 %). In summary, compaction is one of the significant factors that cause reservoir densification in the study area.

5.1.2 Cementation

Cementation is also one of the important diagenetic features which affects the reservoir quality in the Xiahuapidianzi Formation. Nearly all of the Liuhe sandstones underwent various levels of cementation. Mineralogically, there are two kinds of cementation in this area, clay mineral cementation and carbonate mineral cementation. Carbonate mineral (calcite and ferro-calcite) cementation is the most prevalent type of cement in Liuhe sandstones. Fig. 11 indicates an overall negative relationship and clearly suggests that the physical properties of reservoir are controlled by cementation. As shown in Table 3, the content of carbonate mineral and cement in the lower Xiahuapidianzi Formation (>1100 m) is higher than the upper Xiahuapidianzi Formation (<800 m).

5.1.3 Dissolution

Secondary porosity refers to the pore space resulting from the partial to complete dissolution of cements and/or detrital framework grains (Tobin et al., 2010). Dissolution is critical to the formation of secondary pore in sandstone reservoir. However, it is not obvious, and the reservoir is short of secondary porosity in this area. The dissolution porosity ranges from 0.1 to 0.9% and represents < 20% of the total porosity observed in thin section or FE-SEM images (Table 3). Thus,
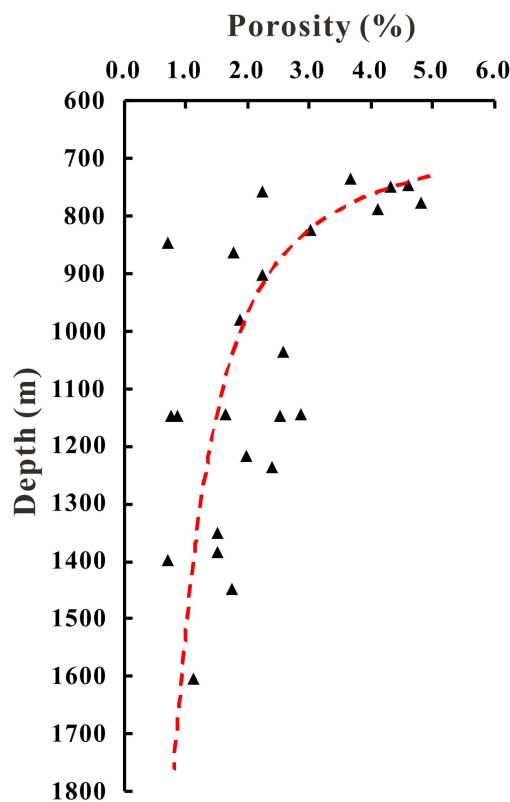

Fig. 10. Vertical distribution of porosity of the tight reservoir in Well LC1 from the Liuhe Basin.

dissolution has a minor impact on the physical properties of the reservoir in improving the reservoir storage capacity.

5.1.4 Quantitative control of diagenesis on porosity

The above-mentioned research focuses on the qualitative controlling factor analysis of the diagenesis (compaction, cementation, dissolution) on the tight reservoir. However, it still cannot completely explain the main issue. Compaction and cementation destroy the pore intensively, while dissolution modify the pore structure.

The original porosity (OP) can be estimated by the following equation (Bread and Weyl, 1973):

$$OP = 20.9 + \frac{22.92}{S_o} \tag{7}$$

where S_o is the sorting coefficient.

The cementational porosity loss (CEPL) can be obtained by statistics method. We propose the area occupied by cement is used to quantitatively evaluate cementational porosity loss. The principle is that the areal cementation of the images in the rock thin section is almost equal to the cementational porosity loss of the rocks. In the same way, the dissolution porosity increase (DIPI) could also be marked by the rock thin section.

Finally, the compactional porosity loss (COPL) can be estimated by equation 52:
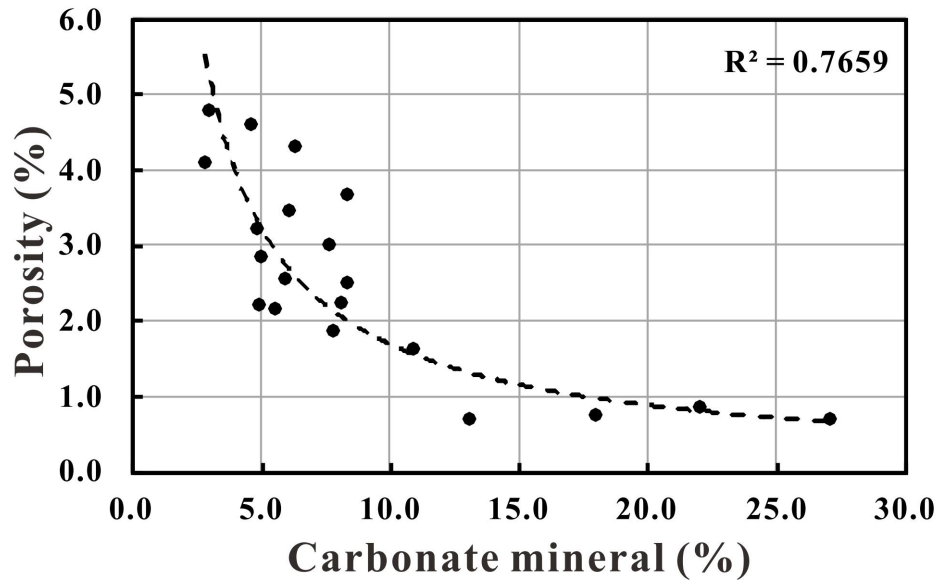
$$COPL = OP + DIPI - CEPL - \Phi_{now} \tag{8}$$

Fig. 11. Relationship between the porosity and carbonate mineral of the tight reservoir in Well LC1 from the Liuhe Basin.
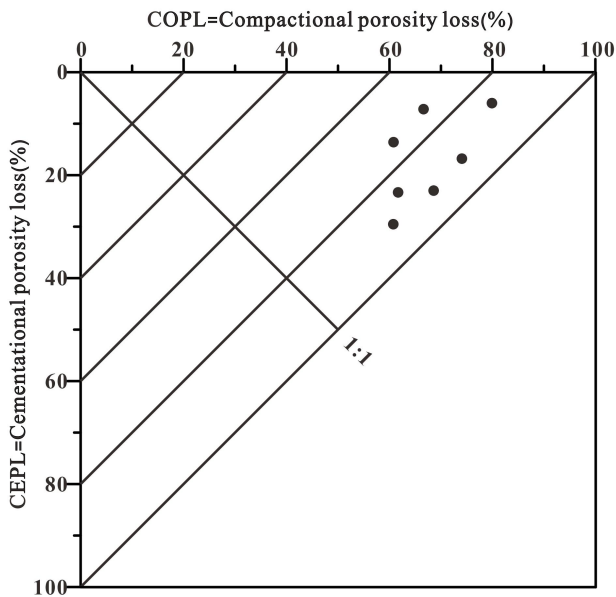

Fig. 12. Plot of compactional porosity loss (COPL) versus cementational porosity loss (CEPL) for 7 sandstone samples.

A plot of corrected COPL versus CEPL reveals that compaction was overall more obvious than cementation in reducing porosity. Most of the porosities have been destroyed by compaction, assuming a more than original 60% depositional porosity (Fig. 12). The greater role of compaction than cementation is attributed to the low composition maturity and the deep burial depth.

5.2 Microfracturing controls on reservoir quality

The lateral extrusion of tectonic stress led to cracks of the brittle rock, connecting pores and providing a good channel for the flow of fluids in the rocks (Zhou and Ji, 2016). Due to the frequent tectonic movements in the study area, especially in the late Cretaceous, microfractures could be produced, which not only improve the reservoir property but also enhance the reservoir storage capacity (Fig. 8g, h).

6. Conclusions

(1) The Liuhe sandstones dominated by lithic arkoses and feldspathic litharenites are tight reservoirs with low porosity ($\Phi < 5\%$). The residual primary intergranular pores provide the primary reservoir space.

(2) Compaction and carbonate cementation are the two decisive mechanisms causing sandstones of the Xiahuapidianzi Formation to lose porosity after deposition. Dissolution of feldspar grains and lithic debris particles is not obvious to improvement in the reservoir physical properties. The microfractures caused by tectonic functions improve the physical properties of the tight sandstone reservoir.

(3) Water film thickness measurements indicate that the theoretical cutoff of porosity is 3.3% in the tight reservoir of Xiahuapidianzi Formation. Tight sandstone reservoirs in the lower Xiahuapidianzi Formation are mainly invalid as most of the measured porosities are less than the theoretical cutoff. The occurrence of effective reservoirs (porosity > 3.3%) is mainly in the upper Xiahuapidianzi Formation due to weak compaction and cementation.

Acknowledgments

References

Abdolmaleki, J., Tavakoli, V., Asadi-Eskandar, A. Sedimentological and diagenetic controls on reservoir properties in the PermianTriassic successions of Western Persian Gulf, Southern Iran. J. Petrol. Sci. Eng. 2016, 141: 90-113.

Ajdukiewicz, J.M., Lander, R.H. Sandstone reservoir quality prediction: The state of the art. Aapg Bull. 2010, 94(8): 1083-1091.

Anders, M.H., Laubach, S.E., Scholz, C.H. Microfractures: A review. J. Struct. Geol. 2014, 69: 377-394.

Aretz, A., Bär, K., Götz, A.E., et al. Outcrop analogue study of Permocarboniferous geothermal sandstone reservoir formations (northern Upper Rhine Graben, Germany): impact of mineral content, depositional environment and diagenesis on petrophysical properties. Int. J. Ear Sci. 2016, 105(5): 1431-1452.

Bao, C. Nature gas geoscience. Beijing: Science press, 1988 (in Chinese).

Beard, D.C., Weyl, P.K. Influence of texture on porosity and permeability of unconsolidated sand. Aapg Bull. 1973, 57(2): 349-369.

Bjørlykke, K., Jahren, J. Open or closed geochemical systems during diagensis in sedimentary basins: Constraints on mass transfer during diagenesis and the prediction of porosity in sandstone and carbonate reservoirs. Aapg Bull. 2012, 96(12): 2193-2214.

Bohr, J., Wogelius, R.A., Morris, P.M., et al. Thickness and structure of the water film deposited from vapour on calcite surfaces. Geochim. Cosmochim. Ac. 2010, 74(21): 5985-5999.

Brunauer, S., Emmett, P.H., Teller, E. Adsorption of gases in multimolecular layers. J. Am. Chem. Soc. 1938, 60(2): 309-319.

Chatterjee, R., Gupta, S.D., Farooqui, M.Y. Application of nuclear magnetic resonance logs for evaluating low-resistivity reservoirs: a case study from the Cambay basin, India. J. Geophys. Eng. 2012, 9(5): 595.

Chatterjee, R., Gupta, S.D., Farroqui, M.Y. Reservoir identification using full stack seismic inversion technique: a case study from Cambay basin oilfields, India. J. Petrol. Sci. Eng. 2013, 109(5): 87-95.

Chatterjee, R., Gupta, S.D., Mandal, P.P. Fracture and stress orientation from borehole image logs: A case study from Cambay basin, India. J. Geol. Soc. India 2017, 89(5): 573-580.

Chen, Y., Wei, L., Mastalerz, M., et al. The effect of analytical particle size on gas adsorption porosimetry of shale. Int. J. Coal. Geol. 2015, 138: 103-112.

Derjaguin, B.V., Churaev, N.V. Structural component of disjoining pressure. J. Colloid Interf. Sci. 1974, 49(2):

249-255.

Dickson, J.A.D. Carbonate identification and genesis as revealed by staining. J. Sediment. Petrol. 1966, 36(2): 491-505.

Dutton, S.P., Loucks, R.G. Diagenetic controls on evolution of porosity and permeability in lower Tertiary Wilcox sandstones from shallow to ultradeep (200-6700 m) burial, Gulf of Mexico Basin, U.S.A. Mar. Petrol. Geol. 2010, 27(1): 69-81.

Folk, R.L. Petrology of sedimentary rocks. Austin: Hemphill Publishing Company, 1980.

Gao, G., Shen, X., Han, Y.L. The physical properties, lowest limit values in sandstone conducting system and their affections to oil accumulation in the setting of low porosity and permeability: taking chang (4+5) and chang 6 sections of yanchang formation in hujianshan area of ordos. Geol. J. China Uni. 2010, 16(3): 351-357 (in Chinese with English abstract).

Ge, X., Fan, Y., Xiao, Y., et al. Quantitative evaluation of the heterogeneity for tight sand based on the nuclear magnetic resonance imaging. J. Nat. Gas Sci. Eng. 2017, 38: 74-80.

Gee, M.L., Healy, T.W., White, L.R. Hydrophobicity effects in the condensation of water films on quartz. J. Colloid Interf. Sci. 1990, 140(2): 450-465.

He, C.Z., Hua, M.Q. The water film thickness in hydrocarbon reservoirs. Petrol. Explor. Dev. 1998, 25: 75-77 (in Chinese with English abstract).

Hillier, S. Quantitative analysis of clay and other minerals in sandstones by XRay powder diffraction (XRPD). Int. Assoc. Sedimentol. Spec. Publ. 2003, 34: 213-251.

Lai, J., Wang, G., Chai, Y., et al. Depositional and diagenetic controls on pore Structure of tight Gas sandstone reservoirs: evidence from lower Cretaceous Bashijiqike Formation in Kelasu Thrust Belts, Kuqa depression in Tarim Basin of West China. Resour. Geol. 2015, 65(2): 55-75.

Lai, J., Wang, G., Fan, Z., et al. Fracture detection in oil-based drilling mud using a combination of borehole image and sonic logs. Mar. Petrol. Geol. 2017, 84: 195-214.

Lan, C., Yang, M., Zhang, Y. Impact of sequence stratigraphy, depositional facies and diagenesis on reservoir quality: A case study on the Pennsylvanian Taiyuan sandstones, northeastern Ordos Basin, China. Mar. Petrol. Geol. 2016, 69: 216-230.

Li, W.H., Zhang, Z., Zan, L., et al. Lower limits of physical properties and their controlling factors of effective coarse-grained clastic reservoirs in the Shahejie Formation on northern steep slope of Bonan subsag, the Bohai Bay Basin. Oil Gas Geol. 2012, 332(s34): 271-277 (in Chinese with English abstract).

Liu, Z., Liu, J.J., Wang, W. Experimental analyses on critical conditions of oil charge for low-permeability sandstones: a case study of Xifeng oilfield, Ordos Basin. Acta Petrol. Sin. 2012, 33: 996-1002 (in Chinese with English abstract).

Maast, T.E., Jahren, J., Bjrlykke, K. Diagenetic controls on reservoir quality in Middle to Upper Jurassic sandstones

in the South Viking Graben, North Sea. Aapg Bull. 2011, 95(11): 1937-1958.

Moore, D.M., Reynolds, R.C. X-ray diffraction and the identification and analysis of clay minerals. Oxford: Oxford University Press, 1989.

Morad, S., Ketzer, J.M., Ros, L.F.D. Spatial and temporal distribution of diagenetic alterations in siliciclastic rocks: implications for mass transfer in sedimentary basins. Sedimentology 2000, 47(s1): 95120.

Nishiyama, N., Yokoyama, T. Does the reactive surface area of sandstone depend on water saturation? - The role of reactive-transport in water film. Geochim. Cosmochim. Ac. 2013, 122: 153-169.

Ou, C.G., Chen, W., Ma, Z.G. Quantitative identification and analysis of Sub-Seismic extensional structure system: technique schemes and processes. J. Geophys. Eng. 2015, 12(3): 502-514.

Paxton, S.T., Szabo, J.O., Ajdukiewicz, J.M., et al. Construction of an intergranular volume compaction curve for evaluating and predicting compaction and porosity loss in rigid-grain sandstone reservoirs. Aapg Bull. 2002, 86(12): 2047-2067.

Shan, X.L., Xie, X.T., Ren, Y. Meso-Cenozoic unconventional hydrocarbon resources in eastern Jilin and prospect of development. Global Geol. 2013, 32(1): 77-83 (in Chinese with English abstract).

Staszczuk, P. Studies of silica gel surface wetting phenomena by means of controlled-rate thermal analysis. Colloid. Surface. A 1995, 105(2-3): 291303.

Taylor, T.R., Giles, M.R., Hathon, L.A., et al. Sandstone diagenesis and reservoir quality prediction: Models, Myths, and reality. Aapg Bull. 2010, 94(8): 1093-1132.

Tobin, R.C., McClain, T., Lieber, R.B., et al. Reservoir quality modeling of tight-gas sands in Wamsutter Field: Integration of diagenesis, petroleum systems, and production. Aapg Bull. 2010, 94(8): 1229-1266.

Tokunaga, T.K. Physicochemical controls on adsorbed water film thickness in unsaturated geological media. Water Resour. Res. 2011, 47(8): W08514.

Wang, D.C., Zhang, R.Q., Shi, Y.H. The basis of hydrogeology. Beijing: Geological Publishing House, 2006 (in Chinese).

Wang, J., Cao, Y.C., Gao, Y.J., et al. Petrophysical parameter cutoff and controlling factors of effective reservoir of red beds sandbodies of Paleogene in Dongying depression. J.

China Uni. Petrol. 2011, 35(4): 27-33 (in Chinese with English abstract).

Wang, P.F., Jiang, Z.X., Ji, W., et al. Heterogeneity of intergranular, intraparticle and organic pores in Longmaxi shale in Sichuan Basin, South China: Evidence from SEM digital images and fractal and multifractal geometries. Mar. Petrol. Geol. 2016a, 72: 122-138.

Wang, Y., Liu, J., Wang, W., et al. The research on the determination of the porosity limitation of the low permeability sandstone reservoirs by the water film thickness. Petrochem. Ind. Appl. 2012, 31: 13-16 (in Chinese with English abstract).

Wu, K.J, Liu, L.F, Xu, Z.J., et al. Lower limits of pore throat radius, porosity and permeability for tight oil accumulations in the Chang7 Member, Ordos Basin. Petrol. Geol. Exper. 2016b, 38: 63-69 (in Chinese with English abstract).

Xu, H.L., Fan, C.Y., Gao, X.J. Early Cretaceous prototype restoration of the basin group in eastern Jilin. Glob. Geol. 2013, 32(2): 263-272 (in Chinese with English abstract).

Yao, Y., Liu, D., Che, Y., et al. Petrophysical characterization of coals by low-field nuclear magnetic resonance (NMR). Fuel 2010, 89(7): 1371-1380.

Zhang, L.C., Lu, S.F., Xiao, D.S., et al. Characterization of full pore size distribution and its significance to macroscopic physical parameters in tight glutenites. J. Nat. Gas Sci. Eng. 2017, 38: 434-449.

Zhang, X.Q., Dai, Z., Liu, L., et al. Application of theory of water film reform the reservoir in tight and permeability sandstone. J. Miner. Petrol. 1998, 18(s1): 161-163 (in Chinese with English abstract).

Zhou, Y., Ji, Y., Zhang, S., et al. Controls on reservoir quality of lower cretaceous tight sandstones in the Laiyang Sag, Jiaolai Basin, Eastern China: Integrated sedimentologic, diagenetic and microfracturing data. Mar. Petrol. Geol. 2016, 76: 26-50.

Zhu, R.K., Xia, Z., Liu, L.H., et al. Depositional system and favorable reservoir distribution of Xujiahe Formation in Sichuan Basin. Petrol. Explor. Dev. 2009, 36(1): 46-55.

Zou, C.N., Zhu, R.K., Bai, B., et al. First discovery of nano-pore throat in oil and gas reservoir in China and its scientific value. Acta Petrol. Sin. 2011, 27(6): 1857-1864.